Evaluating Tensile Rupture Effects in Geogrid-Reinforced Sand Under Triaxial Compression

Arunrassamee, C.[1] Udomsomboon, S.[2] Pinwiset, C.[3] Kongkitkul, W.[4,*] and Silakub, H.[5]

[1,2,3,4,5] Department of Civil Engineering, Faculty of Engineering, King Mongkut's University of Technology Thonburi, Bangkok, THAILAND
**Corresponding author; E-mail address: warat.kon@kmutt.ac.th*

Abstract

This study investigates the influence of tensile rupture in geogrid layers on the compressive failure behavior of reinforced sand. Consolidated drained triaxial compression tests were conducted to compare unreinforced sand with sand reinforced by three evenly spaced layers of biaxial polypropylene geogrid. The research explored sixteen rupture configurations by varying the number of ruptured strands, rupture directions, and layer locations. Results demonstrated that geogrid reinforcement enhances compressive strength even when ruptures occur, although the degree of strength enhancement depends on the rupture pattern. To quantify these effects, the study introduced the rupture fraction (RF) and strength reduction factor (SRF), establishing a clear correlation between them. Furthermore, an isotropic perfectly plastic model accurately predicted the compressive strength of both intact and ruptured reinforced sand, providing a reliable framework for evaluating the performance of geogrid-reinforced systems under rupture conditions.

Keywords: Compressive strength, Geogrid, Reinforced sand, Ruptured geogrid, Triaxial compression test

1. Introduction

Geogrid, a synthetic material engineered for soil reinforcement, has become a staple in improving the stability of earth walls and the foundational layers beneath roads and buildings. This is especially crucial in areas where soil structures are under significant tensile stress. In the realm of geosynthetic-reinforced soil (GRS) structures, geogrids are instrumental in strengthening the backfill soil. This reinforcement enhances the compressive strength of the GRS structure while reducing lateral deformation (Tatsuoka, 2019). When lateral backfill soil is subjected to vertical compression, it undergoes lateral expansion. This expansion activates tensile forces within the geogrid, which then exerts additional confining pressure on the backfill. This dynamic is known as the tensile reinforcing effect, which is central to the stability provided by geogrids.

Research indicates that approximations are crucial for estimating the compressive strength of GRS structures under vertical loads. Plane strain compression (PSC) tests, designed to replicate typical field conditions, have been conducted on air-dried Toyoura sand, both unreinforced and reinforced with various types of materials. Tatsuoka (2004) proposed an approximate closed-form solution for the compressive strength of reinforced soil, which has been used to predict the performance of reinforced sand in these tests. The results align well with predictions, confirming the reliability of this method.

In a recent study, consolidation drained triaxial compression (CDTC) tests were carried out on medium-sized sand specimens to explore the effects of reinforcement tensile rupture on compressive strength. The study compared unreinforced sand specimens with those reinforced by three layers of polypropylene (PP) geogrid. Key factors such as the number and location of rupture layers, as well as the rupture strands, were analyzed to understand how tensile strength loss impacts the overall compressive strength of the reinforced sand.

Table 1 Covering ratio calculated as per the dimensions.

Dimension	Dimension of the geogrid sheet, mm x mm	Number of transverse members	Number of longitudinal members	Transverse member's width, mm	Transverse member's length, mm	Longitudinal member's width, mm	Longitudinal member's length, mm	Covering ratio, %
Secugrid® 60/60 Q1	120 x 120	3	3	9	120	9	120	45.00

2. Test Materials

In the triaxial compression test, samples were prepared using air-dried sand, both unreinforced and reinforced. The properties of the materials used in sample preparation are as follows:

2.1 Sand

In this study, we explored the properties of KMUTT sand, a material characterized by its specific particle size range. This sand features particles that are fine enough to pass through sieve No. 4 but are retained on sieve No. 100. With a specific gravity (G_s) of 2.64 and a mean particle diameter (D_{50}) of 0.285 mm, KMUTT sand offers a unique profile. Additionally, it has a coefficient of uniformity (C_u) stands at 1.87, while its coefficient of curvature (C_c) measures 0.94. The sand also presents a maximum void ratio (e_{max}) of 1.042 and a minimum void ratio (e_{min}) of 0.681, providing valuable insights into its compaction and density characteristics.

2.2 Geogrid

In this study, the effectiveness of polypropylene (PP) geogrids in reinforcing soil structures under triaxial compression tests. Geogrids are instrumental in enhancing the stability, safety, and durability of soil formations by reducing deformation. For this investigation, we utilized a biaxial geogrid—specifically, the Secugrid® 60/60 Q1 as shown in Fig. 1. This geogrid, made from extruded and drawn PP bars that are laid and welded together, offers robust and reliable reinforcement. The dimensions of the geogrid are 120 mm by 120 mm, and it boasts a tensile strength (T_{ult}) of 60 kN/m. In addition, Table 1 lists the covering ratio.

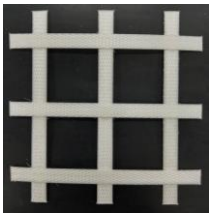

Fig. 1 Geogrid specimens used to reinforce sand in triaxial

3. Methodology

3.1 Sample preparation method

The initial step in preparing the sample involves lubricating the upper and lower heads of the sample with high-vacuum silicone grease. This lubrication ensures that the sample can be easily handled and manipulated. Following lubrication, a suitable membrane is cut to size and placed on the base of the mold. The other end of the membrane is then inserted into the assembled mold. It is important to cover the end of the membrane at the top of the mold's opening. A suction force is applied to secure the membrane against the inner surface of the mold, ensuring a tight fit. The membrane is then adjusted to align within the specified boundary and along the edge of the sample.

Filling the mold with sand requires careful control to achieve the desired density and uniformity. This is accomplished by using a multiple-sieving pluviating machine, which helps regulate the sand's density. In this study, the relative density (D_r) of the prepared sample was found to be approximately 90-95 percent. For samples that require reinforcement, the sand level should be slightly higher than the target level. Any excess sand should be removed to achieve the correct height.

The next step involves placing a reinforcing mesh on top of the prepared sand at the designated level. Sand is then sprinkled over the mesh, followed by compaction using a rubber hammer and a log. This compaction process helps to remove loose sand from within the mesh opening. This procedure is repeated for each additional layer of reinforcement until the desired number of layers is achieved.

Upon preparing the final layer of sand, the top cover is attached to the sample. The end of the membrane is wrapped around the top cover, and the sample is sealed to prevent any leakage. Suction force on the mold is then reduced to zero. A

suction force is applied through the pipe located at the top cover and base, maintaining a constant value of -30 kPa throughout the test. Finally, the mold is removed, and the prepared sample is ready for testing.

3.2 Test method

After preparing the sample, the shaft of the compression cell is mounted onto the press machine. A load cell on the top cover measures the force exerted on the sample, while vertical and horizontal deformations are monitored using a displacement transducer (DT) and two laser displacement sensors (LDS), respectively. Additionally, a pressure transducer records the clamping pressure. Following the installation and calibration of these devices, the sample is compressed at a rate of 0.3 mm/min until failure as shown in Fig. 2, allowing for the accurate collection of data on the material's response under stress.

3.3 Stress and strain parameters

The following definitions of stress and strain parameters are used in this study:

Deviator stress (q) can be defined as shown in Eq. (1).

$$q = \frac{F}{A_0} \tag{1}$$

where, F is the axial load (measured by the load cell) (kN), and A_0 is the initial cross-section area (m^2)

This research presents the compressive strength of reinforced sand using the average stress ratio (R) parameter which is defined as shown in Eq. (2).

$$R = \frac{\sigma_1}{\sigma_3} = \frac{\sigma_c + q}{\sigma_c} = \frac{\sigma_c + \frac{F}{A_0}}{\sigma_c} \tag{2}$$

where, q = deviator stress (kPa) determined as withEq 3.1 and σ_c = confining pressure (30 kPa)

The vertical deformation of the sample represented by the vertical strain (ε_v) can be defined as shown in Eq. (3).

$$\varepsilon_v = -\frac{\Delta H}{H_0} x100(\%) \tag{3}$$

where, ΔH = change in height of specimen (mm) (measured by a DT) and H_0 = initial height of specimen (mm) (240 mm)

$$\varepsilon_h = -\frac{(\Delta B_1 + \Delta B_2)}{B_0} x100(\%) \tag{4}$$

Horizontal strain (ε_h) can be defined as shown in Eq. (4).

where, ΔB_1 = change in width of specimen on left side (mm) (measured by 1st LDS), ΔB_2 = change in width of specimen on right side (mm) (measured by 2nd LDS) and B_0 = initial width of specimen (mm) (120 mm)

Fig. 2 Triaxial compression specimen during shearing process

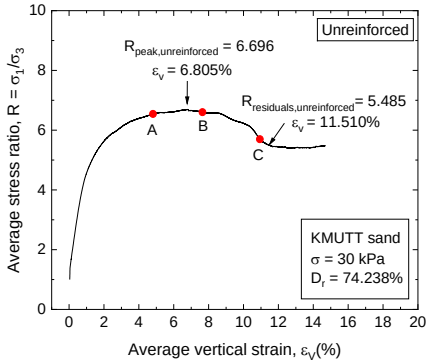

Fig. 3 Relationship between average stress ratio (R) and average axial strain (ε_v) from a triaxial compression test on unreinforced sand

4. Results and discussions

4.1 Unreinforced sand specimen

Figure 3 shows the relationship between the average stress ratio (R) and average vertical strain (ε_v) from a triaxial compression test on unreinforced sand. The graph reveals an initial rapid increase in the R value, followed by a deceleration before reaching the maximum stress ratio (R_{peak}) of 6.696, corresponding to a vertical strain of 6.805%. Subsequently, during the residual stage at the R value at the start of residual state where R is rather constant with increasing ε_v ($R_{residual}$) of 5.485, with a vertical strain of 11.510%.

$$\phi = \sin^{-1}\left(\frac{R-1}{R+1}\right) \tag{5}$$

These values, R_{peak} and $R_{residual}$, facilitate the calculation of the friction angle (ϕ) using the formula can be defined as shown in Eq. (5), assuming zero cohesion (c).

The friction angles are equal to 47.743° for peak state (ϕ_{peak}) and 43.755° for the residual state ($\phi_{residual}$).

4.2 Unreinforced sand specimen

Figure 4-7 compares the relationship between the average stress ratio (R) and average vertical strain (ε_v) between the fully reinforced and unreinforced sand specimens under various conditions. The unreinforced sand achieves a maximum stress ratio ($R_{peak,unreinforced}$) of 6.696, while the fully reinforced sand, featuring a non-ruptured geogrid layer, reaches a higher maximum stress ratio ($R_{peak,fully}$) of 12.536. This indicates that reinforcement significantly improves the stress ratio, with the geogrid layer enhancing local confining pressure within the sand. The marked difference in R_{max} values underscores the effectiveness of reinforcement in increasing the sand's load-bearing capacity as shown in table 2.

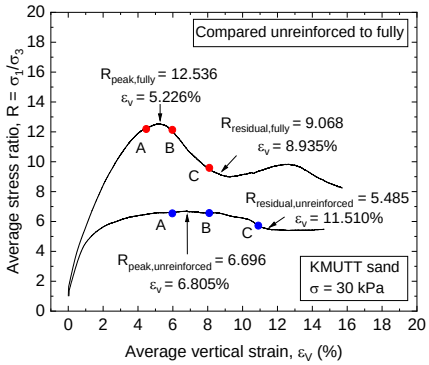

Fig. 4 Comparison of relationships between R and ε_v between fully reinforced sand and unreinforced sand specimens

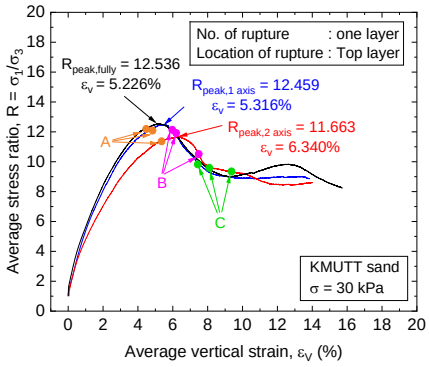

Fig. 5 Comparison of R-ε_v relationships between fully reinforced sand and 1-layer ruptured reinforced sands (one and two axes)

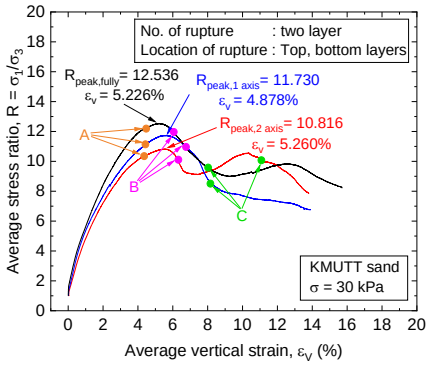

Fig. 6 Comparison of R-ε_v relationships between fully reinforced sand and 2-layer ruptured reinforced sand (one and two axes)

Table 2 Summary of the R_{max}, ε_v and ε_h when R = R_{max} of unreinforced sand and sand reinforced with various geogrid types

No	Test Name	Maximum vertical stress (kPa)	Peak				Residual			
			R	ε_v (%)	ε_h (%)	Friction angle (°)	R	ε_v (%)	ε_h (%)	Friction angle (°)
1	Unreinforced	172.168	6.696	6.805	4.205	47.743	5.485	11.510	14.874	43.755
2	Fully reinforced	348.906	12.532	5.226	3.922	58.452	9.068	8.935	10.482	53.259
3	1-TL-XMS	343.776	12.459	5.316	4.253	58.364	9.072	8.632	11.308	53.267
4	1-ML-XMS	325.523	11.718	5.253	5.073	57.431	8.867	7.607	12.723	52.874
5	1-BL-XMS	321.875	11.897	4.938	4.077	57.664	10.640	6.698	4.577	55.912
6	2-TBL-XMS	318.714	11.580	5.260	3.170	57.248	9.567	9.667	4.527	54.167
7	2-TML-XMS	322.598	11.730	5.555	6.081	57.446	7.929	9.040	11.524	50.897
8	2-MBL-XMS	319.728	11.637	5.413	5.657	57.323	8.997	10.261	7.059	53.124
9	3-TMBL-XMS	302.767	11.010	5.797	5.201	56.457	6.923	11.236	15.698	48.381
10	3-TMBL-XYMS	290.778	10.626	5.377	6.027	55.890	8.506	10.651	10.103	52.148
11	1-TL-XYMS	322.332	11.662	6.340	6.272	57.356	8.633	11.293	16.419	52.408
12	1-ML-XYMS	303.812	11.071	5.024	5.678	56.545	9.489	6.590	8.541	54.030
13	1-BL-XYMS	296.853	10.780	4.366	3.098	56.122	7.621	8.643	3.236	50.176
14	2-TBL-XYMS	293.969	10.684	4.878	3.102	55.979	6.906	9.511	5.087	48.334
15	2-TML-XYMS	295.445	10.816	5.280	6.192	56.175	9.280	6.705	8.646	53.653
16	2-MBL-XYMS	292.768	10.771	5.273	5.153	56.108	9.411	6.598	5.016	53.892

4.3 Effects of rupture in geogrids on the maximum stress ratio

The study demonstrates that sand specimens reinforced with geogrid layers and ruptured in one direction achieved the highest maximum stress ratio, with fully reinforced sand exhibiting the greatest value. The effectiveness of geogrid reinforcement decreases slightly when the rupture occurs in multiple directions. Sand specimens with geogrid layers ruptured in one direction exhibited the highest R_{max} value, denoted as $R_{max,fully}$, reaching a maximum stress ratio of 12.536.

The position and number of rupture directions in geogrid layers significantly impact R_{max} values. A single rupture in one direction typically results in a higher R_{max} compared to multiple ruptures in different directions. The aggregated data, as shown in Figure 8, shows the average R_{max} values for different numbers of ruptured layers, with the graph differentiating between one and two rupture directions. This consistent trend across tests highlights that R_{max} generally decreases as the number of ruptured locations increases, providing a valuable reference for future predictions.

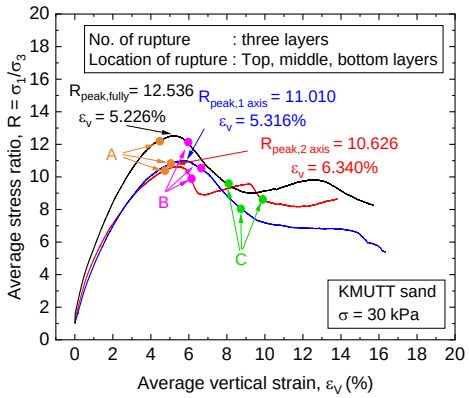

Fig. 7 Comparison of R-ε_v relationships between fully reinforced sand and 3-layer ruptured reinforced sands

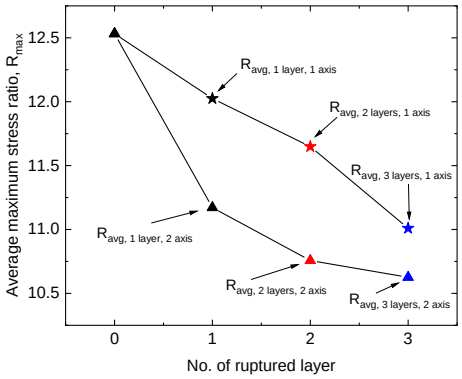

Fig. 8 Relationship between R_{max} and number of ruptured layer averaged respectively for the ruptures in one and two directions

4.4 Assembling the impact of geogrids ruptures on strength reduction factor

The relationship between the strength reduction factor (SRF) and ruptured fraction (RF) is shown in Figure 9. To determine RF, the number of ruptured geogrid locations was divided by the total number of geogrid stands. The SRF was derived by dividing the maximum average stress ratio for each case by the ratio for the fully reinforced specimen. The SRF value is plotted against RF establish the trend of the SFR across the RF value. The trend line is fitted using the formula $y = ax^b$, where x represents the RF. The analysis of SRF relative to RF reveals a clear trend, showing how the SRF decreases as the RF increases, with the maximum RF corresponding to an SRF of 0.534, derived from an unreinforced sand R_{max} of 6.696, which results in the SRF as shown in Eq. (6).

$$SRF = 1 - 0.474(RF)^{0.72} \quad (6)$$

The trend line fitted to the data highlights a predictable relationship, which is crucial for understanding the performance of reinforced sand in various conditions.

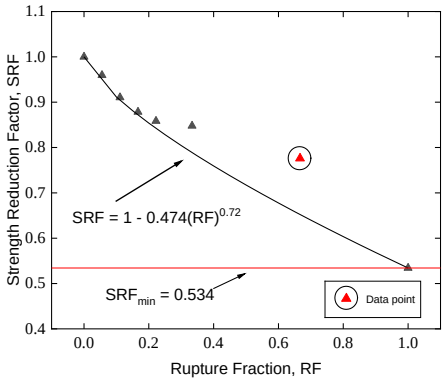

Fig. 9 Relationship between SRF and RF

5. Approximation of the compressive strength of geogrid-reinforced sand with rupture

The tests compared predicted maximum resistance (R_{max}), adjusted by the strength reduction factor (SRF), with actual results. Tatsuoka (2004) method for predicting compressive strength identified two key factors: progressive failure of sand can increase compressive strength even after stress ratios decrease, and higher local confining pressure reduces the peak friction angle. These insights are crucial for accurate predictions of compressive strength under varying conditions.

5.1 Interface friction angle between sand and geogrid

According to Peng et al. (2000), the interface friction angle (μ) between sand and geogrid at a covering ratio (CR) of 100% ($\mu_{CR=100\%}$) was 31.3025°. The μ values corresponding to CRs less than 100% were obtained through 2D FEM analysis, and the resulting μ–CR relationship is illustrated in Figure 10. Later, Kongkitkul and Tatsuoka (2006) normalized μ at any CR by $\mu_{CR=100\%}$ and proposed a relationship between $\mu/\mu_{CR=100\%}$ and CR, as shown in Figure 11. Consequently, for cases where $\mu_{CR=100\%}$ differs from the value reported by Peng et al. (2000), the μ corresponding to a given CR can still be determined using the normalized relationship in Figure 11.

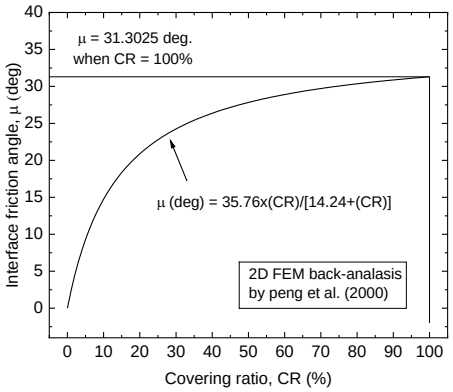

Fig. 10 Relationship between μ and CR for $\mu_{CR=100\%}$ = 31.3025 deg. obtained from 2D FEM analysis by Peng et al. (2000)

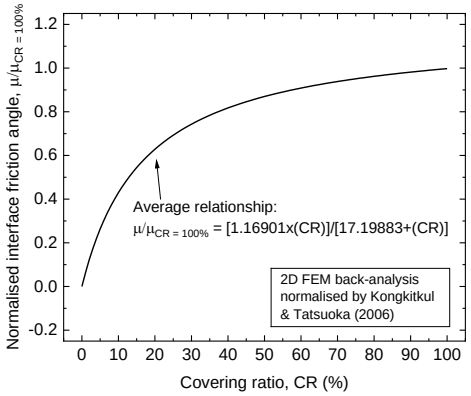

Fig. 11 Relationship between normalized interface friction ($\mu/\mu_{CR=100\%}$) and covering ratio (CR), as proposed by Kongkitkul and Tatsuoka (2006)

5.2 Prediction of compressive strength

Tatsuoka (2004) proposed equations to predict the compressive strength of reinforced soil, including the maximum average stress ratio (R_{max}), which can be calculated using Eqs. (7.1 – 7.5).

$$\bar{R}_{max} = \frac{P_1\left[1-(h/d)\tan\varepsilon\right]+1}{(\tan\varepsilon)^2} \quad (7.1)$$

$$P_1 = \frac{\exp(B)-1}{B} - 1 \quad (7.2)$$

$$B = 2\delta_b\left(\frac{\cos\delta_b+\sin\phi}{\cos\phi}\right)\tan\phi\left(\frac{d}{h}-\tan\varepsilon\right) \quad (7.3)$$

$$\delta_b = \frac{1}{2}\left[\mu+\arcsin\left(\frac{\sin\mu}{\sin\phi}\right)\right] \quad (7.4)$$

$$\varepsilon = \frac{\pi}{4}-\frac{\phi}{2} \quad (7.5)$$

This study focused on determining the coefficient of friction (μ) for geogrid-reinforced sand. It was calculated by examining the relationship between the normalized coefficient of friction $\mu_{CR=100\%}$and the covering ratio, which was found to be 21.95%. According to Peng et al., the μ value for a covering ratio (CR) of 100% is 31.3025 degrees. The results indicate that the predicted curve significantly exceeds the measured R_{max}. Figure 12 reveals that the closest ϕ value is consistently lower than the residual value, thus it was utilized to calculate the predicted R_{max}.

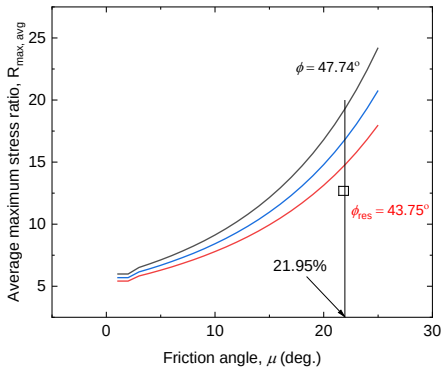

Fig. 12 Relationship between R_{max} and μ predicted by approximate solutions

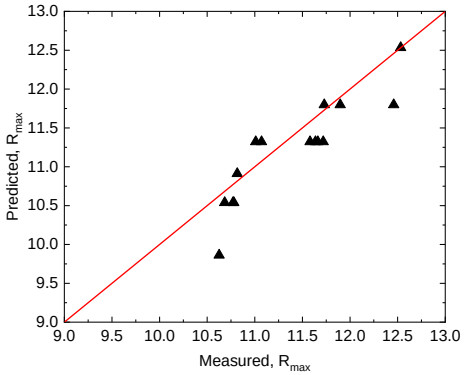

Fig. 13 Comparison of measured and predicted stress ratio

The study successfully established a method for predicting the maximum stress ratio (R_{max}) for geogrid-reinforced sand by calculating the coefficient of friction and using it alongside the covering ratio and other relevant variables. The predicted values were validated against the measured data, showing a higher predicted curve, which suggests the method's reliability.

Table 3 presented the reduction strength factor and fraction of rupture, derived from the relationship between the reduced maximum stress ratio and the predicted maximum stress ratio. Figure 13 illustrated the comparison of the maximum stress ratios.

Despite the generally good agreement between predicted and measured compressive strengths, some discrepancies are evident, as shown in Table 3 and Figure 13. These differences may result from the simplifications in the predictive model, assumptions regarding interface friction, and the non-linear behavior of the reinforced sand. Further refinement of the prediction approach is recommended for improved accuracy in future studies.

Table 3 List of predicted and measure R_{max} values of geogrid-reinforcement sand

No	Test name	R_{test}	Fraction rupture	Reduce factor	$R_{predict}$
1	Completely	12.532	-	-	12.533
2	1-TL-XMS	12.459	0.056	0.941	11.798
3	1-ML-XMS	11.718	0.056	0.941	11.798
4	1-BL-XMS	11.897	0.056	0.941	11.798
5	2-TBL-XMS	11.580	0.111	0.903	11.322
6	2-TML-XMS	11.730	0.111	0.903	11.322
7	2-MB-XMS	11.637	0.111	0.903	11.322
8	3-TMBL-XMS	11.010	0.167	0.871	10.912
9	3-TMBL-XYMS	10.626	0.333	0.787	9.862
10	1-TL-XYMS	11.662	0.111	0.903	11.322
11	1-ML-XYMS	11.071	0.111	0.903	11.322
12	1-BL-XYMS	10.780	0.111	0.903	11.322
13	2-TBL-XYMS	10.684	0.222	0.841	10.538
14	2-TML-XYMS	10.816	0.222	0.841	10.538
15	2-MBL-XYMS	10.771	0.222	0.841	10.538
16	Reference	9.7247	0.667	0.649	8.134

6. Conclusions

In recent studies, geogrid-reinforced sand was found to exhibit significantly higher compressive strength compared to unreinforced sand. This improvement was largely due to the additional confining pressure provided by the tensile strength of the geogrid, which enhanced the soil's load-bearing capacity. The analysis also showed that the pattern and extent of geogrid rupture had a notable effect on the compressive strength. Specifically, an increase in the number of rupture locations or the rupture fraction led to a decrease in compressive strength. Additionally, Tatsuoka's (2004) isotropic perfectly plastic solution, when used in conjunction with the SRF-RF relationship proposed in the study, effectively predicted the compressive strength of sand specimens reinforced with ruptured geogrid layers.

Acknowledgement

Sincere thanks go to NAUE GmbH & Co. KG for supplying the essential geogrid materials. Additionally, the author thanks the Department of Civil Engineering at King Mongkut's University of Technology Thonburi for funding the research.

References

[1] Kongkitkul, W. and Tatsuoka, F. (2006). Compressive Strength of Reinforced Sand in Plane Strain Compression and Its Approximate Solution. *The 8th International Conference on Geosynthetics (8ICG)*, Chiba, Japan, pp. 278-8510.

[2] Kongkitkul, W., Tatsuoka, F., and Hirakawa, D. (2007). Effects of Geosynthetic Reinforcement Type on The Strength and Stiffness of Reinforced Sand in Plane Strain Compression. *Soils and Foundations*, Vol. 47, No. 6, pp. 1109-1122.

[3] Kongkitkul, W., Tatsuoka, F., and Hirakawa, D. (2007). Effects of Reinforcement Type and Loading History on The Deformation of Reinforced Sand in Plane Strain Compression. *Soils and Foundations*, Vol. 47, No. 2, pp. 395-414.

[4] Kongkitkul, W., Tatsuoka, F., and Hirakawa, D. (2007). Rate-Dependent Load-Strain Behaviour of Geogrid Arranged in Sand Under Plane Strain Compression. *Soils and Foundations*, Vol. 47, No. 3, pp. 473-491.

[5] Sumanuschai, O. (2019). *Effects of Tensile Strength and Spacing of Geogrids on the Compressive Strength and Deformation of Reinforced Sand.* M. Eng. Thesis, Department of Civil Engineering, King Mongkut's University of Technology Thonburi, pp. 1-255.

[6] Sumanuschai, O. and Kongkitkul, W. (2020). Effects of Tensile Strength and Spacing of Biaxial Geogrids on the Compressive Strength and Deformation of Reinforced Sand. *The 25th National Convention on Civil Engineering*, July 15-17, 2020, Chonburi, THAILAND.

[7] Tatsuoka, F. (1985). On the Angle of Interface Friction for Cohesionless Soils. *Soils and Foundations*, Vol. 25, No. 4, pp. 135-141.

[8] Tatsuoka, F. (2004). An Approximate Isotropic Perfectly Plastic Solution for Compressive Strength of Geosynthetic-Reinforced Soil. *Geosynthetics International*, Vol. 11, No. 5, pp. 390-405.

[9] Tatsuoka, F. (2019) Geosynthetic-Reinforced Soil Structures for Railways and Roads: Development from Walls to Bridges. *Innovative Infrastructure Solutions*, Vol. 4, pp. 49-67.